

Article

Highly Biocompatible Hemoglobin-Stabilized Gold Nanoparticles for an Enhanced Catalytic Reduction of 4-Nitrophenol

Yanshuai Cui ^{1,*}, Shukai Li ², Ning Yu ³, Xiaodong Yu ¹, Xianbing Ji ¹ and Longgang Wang ²

¹ Hebei Key Laboratory of Agroecological Safety, Department of Environmental Engineering, Hebei University of Environmental Engineering, Qinhuangdao 066102, China; yuxdhy@163.com (X.Y.); jixianbing@hebeuee.edu.cn (X.J.)

² College of Environmental and Chemical Engineering, Yanshan University, Qinhuangdao 066004, China; lishukai1998@163.com (S.L.); lgwang@ysu.edu.cn (L.W.)

³ Qinhuangdao Environment Monitoring Center, Qinhuangdao 066003, China; 18333569079@163.com

* Correspondence: cuiyanshuai09@163.com

Abstract: 4-nitrophenol (4-NP) is a frequently encountered toxic phenolic organic pollutant in water. It is important to develop a simple method to treat 4-NP. Small and monodispersed gold nanoparticles often have good catalytic performance of 4-NP. Hemoglobin (Hb) is a kind of common and important protein in organisms. Herein, highly biocompatible bovine hemoglobin-stabilized gold nanoparticles (Au_n-Hb NPs) were synthesized using hemoglobin as a biological template. Then, the size, zeta potential, and composition of Au_n-Hb NPs were investigated by transmission electron microscopy, dynamic light scattering, and X-ray photoelectron spectroscopy. The Au_n-Hb NPs with small gold nanoparticles of about 1.4–2.4 nm had good catalytic capabilities in reducing 4-NP to form 4-aminophenol. Au₂₀-Hb NPs demonstrated superior catalytic efficiency in the reduction of 4-NP when compared to other nanoparticles. Moreover, as-synthesized Au₂₀-Hb NPs exhibited excellent biocompatibility through the MTT experiment. The method of preparation of gold nanoparticles offers one way to prepare metal nanoparticles for good potential catalytic applications of gold nanoparticles.

Keywords: 4-nitrophenol; hemoglobin; gold nanoparticles; biocompatible; catalysis



Citation: Cui, Y.; Li, S.; Yu, N.; Yu, X.; Ji, X.; Wang, L. Highly Biocompatible Hemoglobin-Stabilized Gold Nanoparticles for an Enhanced Catalytic Reduction of 4-Nitrophenol. *Inorganics* **2024**, *12*, 136. <https://doi.org/10.3390/inorganics12050136>

Academic Editor: Christelle Hureau

Received: 6 March 2024

Revised: 30 April 2024

Accepted: 2 May 2024

Published: 5 May 2024



Copyright: © 2024 by the authors. Licensee MDPI, Basel, Switzerland. This article is an open access article distributed under the terms and conditions of the Creative Commons Attribution (CC BY) license (<https://creativecommons.org/licenses/by/4.0/>).

1. Introduction

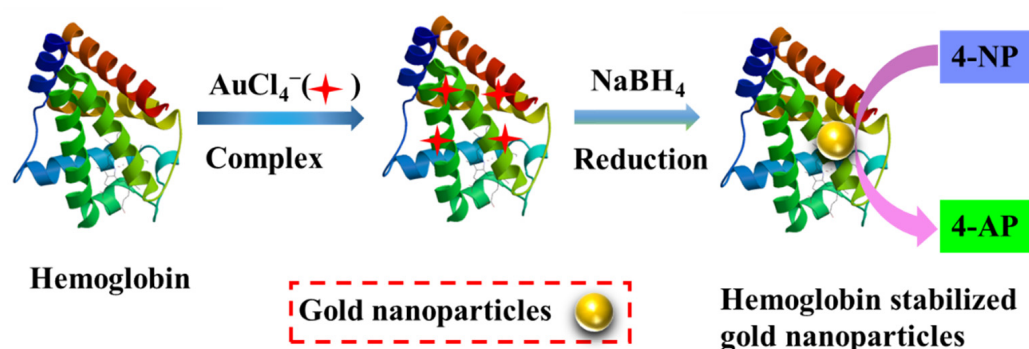
In recent years, nitrophenol compounds as water pollutants seriously threaten people's health and safety [1]. For example, 4-nitrophenol (4-NP) is a very toxic phenolic compound [2]. The concentration of phenolic compounds is strictly controlled in China. Catalytic reduction of 4-NP is one method to eliminate its environmental impact. The resulting compound from the catalytic reduction of 4-NP is known as 4-aminophenol (4-AP) [3]. 4-AP plays a vital role in the manufacturing process of fine chemicals like dyes, pharmaceuticals, and pesticides. The efficiency of converting 4-NP to 4-AP is closely linked to the choice of catalysts. Many nanomaterials such as gold nanoparticles (Au NPs) [4], palladium nanoparticles [5], Cu/Fe nanocomposite [6], and Fe₃O₄@C nanoparticles [7] have been developed to reduce 4-NP. Noble metal nanoparticles with small particle sizes and monodispersed states have good catalytic performance in the 4-NP reduction. However, the noble metal nanoparticles easily aggregate.

The development of nanotechnology in recent years has provided new insights and opportunities for the design of small particle sizes and monodispersed catalysts. Some organic polymers are often used as stabilizers to control the particle size and monodispersed state. There are many options for the use of stabilizers, including polyvinyl pyrrolidone (PVP) and polyethyleneimine (PEI) [5]. Recently, the exploration of an efficient and biocompatible catalyst to treat 4-NP has attracted widespread attention. The use of biocompatible

substances is good for overcoming this problem. Many biocompatible molecules have been used to stabilize the noble metal nanoparticles. He et al. [8] employed sericin as the reducing agent for silver ions, as well as the dispersing and stabilizing agent for the composite of sericin–silver nanoparticles, which exhibited favorable size distribution and maintained long-term stability. Nogueira et al. [9] used cashew gum-hydrolyzed collagen, kappa carrageenan-hydrolyzed collagen, and agar-hydrolyzed collagen as effective nanoparticle stabilizers to prepare silver nanoparticles, respectively. San et al. [10] used three proteins: aminopeptidase PepA, serine endoprotease DegP, and Clp protease to prepare platinum nanoparticles. Bitter gourd polysaccharide, elm pod polysaccharide, and lentinan were also used to stabilize noble metal nanoparticles [11,12]. Large-ring cyclodextrins were also used to stabilize gold nanoparticles in an aqueous phase [13–15]. However, some proteins and polysaccharides have high prices, which is not good for the preparation of noble metal nanoparticles on a large scale.

Bovine hemoglobin is a kind of natural protein found in the blood of bovine. Bovine hemoglobin has an important impact on the survival of the organism. Hemoglobin is a protein composed of four subunits, each consisting of a globin molecule and a heme group. The globin molecule is made up of a chain of amino acids folded into a specific three-dimensional structure, while the heme group contains an iron ion coordinated within a porphyrin ring [16,17]. Bovine hemoglobin functions in the transport of oxygen and carbon dioxide, as well as in regulating the blood's acid–base equilibrium. The bovine hemoglobin extracted from bovine blood is a good ideal metal stabilizer because of its affordable price, good stability, and environmental friendliness. In addition, Au NPs, as a kind of noble metal nanoparticles, are stable in their zero-valence state. Au NPs find extensive application across a spectrum of catalytic processes; they have good catalytic capabilities in the reduction of 4-NP.

In this study, in order to reduce the pollution caused by nitrophenol compounds in the environment, bovine hemoglobin was used to stabilize gold nanoparticles (Scheme 1). We prepared bovine hemoglobin-stabilized gold nanoparticles (Au_n-Hb NPs) with small particle sizes by a facile method. The prepared gold nanoparticles inside Au_n-Hb NPs had a huge specific surface area originating from their small particle size, which was very beneficial for catalyzing 4-NP. Moreover, the biocompatibility and stability of the gold nanoparticles had been greatly improved with the assistance of bovine hemoglobin. Thus, Au_n-Hb NPs demonstrated effective catalysis in the reduction of 4-NP. Overall, we prepared highly biocompatible bovine hemoglobin-stabilized gold nanoparticles for catalytic reduction of 4-NP. The method in this report is good for the development of catalysts in the degradation of nitrophenol compounds.



Scheme 1. The preparation of bovine hemoglobin-stabilized gold nanoparticles and their catalysis application.

2. Results and Discussion

2.1. UV-Vis Spectra Analysis

The bovine hemoglobin solution and HAuCl_4 solution were mixed together for 15 min. Then, the HAuCl_4 solution was reduced by reducing agent NaBH_4 , and bovine hemoglobin was used to stabilize the generated gold nanoparticles. The samples of the bovine hemoglobin solution, HAuCl_4 solution, and $\text{Au}_n\text{-Hb}$ NP solution were measured by a UV-Vis spectrometer with a wavelength from 200 to 600 nm. As shown in Figure 1a, the bovine hemoglobin solution and HAuCl_4 solution had characteristic peaks at 406 nm and 306 nm, respectively. After the preparation of $\text{Au}_n\text{-Hb}$ NPs, the characteristic peaks at 306 nm for the HAuCl_4 solution disappeared, and the characteristic peaks at 406 nm for the bovine hemoglobin solution were greatly reduced. These results indicated that AuCl_4^- was completely reduced to form Au NPs, and Au NPs were complexed within bovine hemoglobin. In addition, the absorbance of the $\text{Au}_n\text{-Hb}$ NPs solution gradually increased with a n -value from 20 to 40, indicating that the amount of Au NPs in the $\text{Au}_n\text{-Hb}$ NPs continued to increase. The color of the $\text{Au}_n\text{-Hb}$ NP ($n = 20, 30, 40$) solution gradually deepened based on the same concentration of bovine hemoglobin, as shown in Figure 1b. Taken together, all the results suggested that we successfully prepared $\text{Au}_n\text{-Hb}$ NPs.

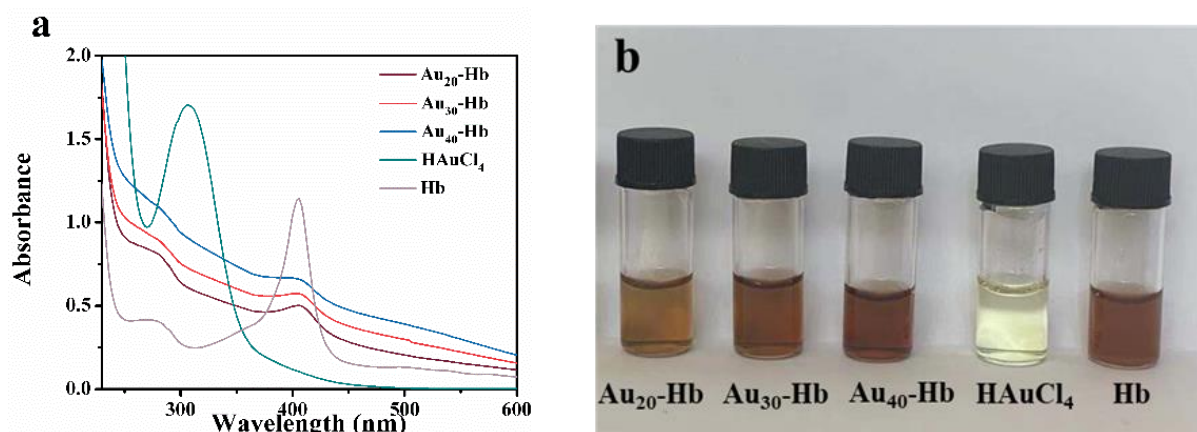


Figure 1. (a) UV-Vis spectra and (b) solutions of $\text{Au}_{20}\text{-Hb}$ NPs, $\text{Au}_{30}\text{-Hb}$ NPs, $\text{Au}_{40}\text{-Hb}$ NPs, HAuCl_4 , and bovine Hb, respectively.

2.2. TEM Observation

The size of nanomaterials plays a crucial role in determining their catalytic efficiency. Herein, the particle size and dispersion condition of $\text{Au}_n\text{-Hb}$ NPs were determined by TEM. Figure 2 shows TEM images of $\text{Au}_n\text{-Hb}$ NPs prepared using bovine hemoglobin with different HAuCl_4 contents. TEM images indicated that $\text{Au}_n\text{-Hb}$ NPs ($n = 20, 30, 40$) had highly dispersed states. The sizes of $\text{Au}_n\text{-Hb}$ NPs were 1.4 ± 0.6 nm for $\text{Au}_{20}\text{-Hb}$ NPs, 2.1 ± 0.6 nm for $\text{Au}_{30}\text{-Hb}$ NPs, and 2.4 ± 0.8 nm for $\text{Au}_{40}\text{-Hb}$ NPs, respectively. The specific surface area of Au NPs inside $\text{Au}_{20}\text{-Hb}$ NPs, $\text{Au}_{30}\text{-Hb}$ NPs, and $\text{Au}_{40}\text{-Hb}$ NPs was 4.3 nm^{-1} , 2.9 nm^{-1} , and 2.5 nm^{-1} , respectively. The Au NPs inside $\text{Au}_n\text{-Hb}$ NPs have small and monodisperse states. It can also be seen that the molar ratio of HAuCl_4 to hemoglobin affects the size of Au NPs. The average diameter of Au NPs inside $\text{Au}_n\text{-Hb}$ NPs increases with the molar ratio of HAuCl_4 to bovine hemoglobin, and the shape of Au NPs remains basically unchanged. Thus, $\text{Au}_n\text{-Hb}$ NPs were characterized by their small size and uniform size distribution, which is beneficial to their catalytic performance.

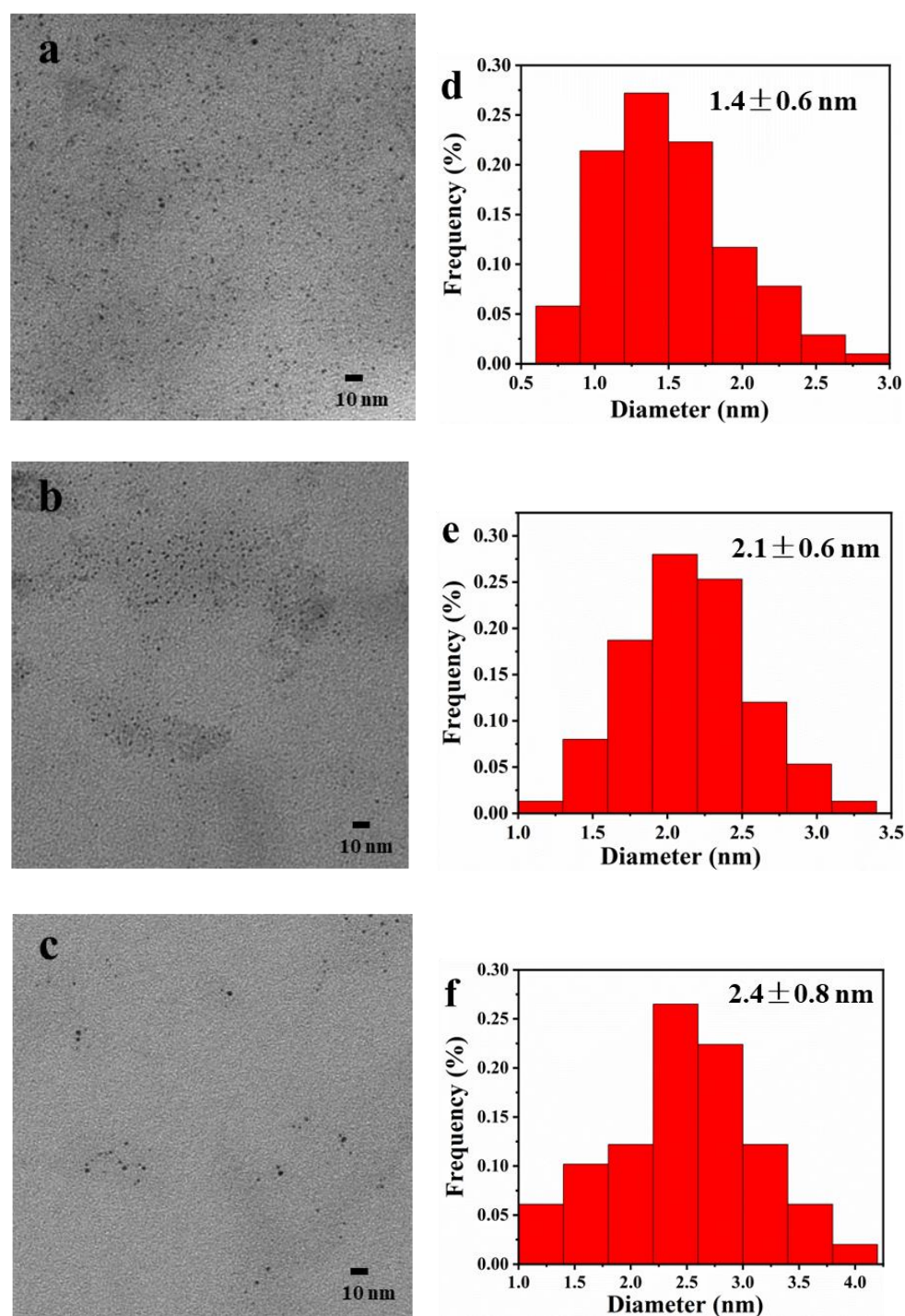


Figure 2. TEM images and corresponding Au NP diameter distribution: (a,d) Au₂₀-Hb NPs, (b,e) Au₃₀-Hb NPs, (c,f) Au₄₀-Hb NPs.

2.3. XPS Analysis

XPS analysis was utilized for further examination of the composition and valence state of the synthesized Au₂₀-Hb NPs. As shown in Figure 3a, the binding energies of about 531.3, 399.7, and 284.6 eV were indexed to O 1s, N 1s, and C 1s, respectively. These elements were derived from bovine hemoglobin. There is little Fe 2p_{3/2} in the XPS survey spectrum of Au₂₀-Hb NPs. To further determine the gold valence, the peaks of Au 4f_{7/2} and Au 4f_{5/2} were observed at 83.92 and 87.64 eV in the high-resolution XPS spectrum of the Au 4f region, as shown in Figure 3b, respectively. The gap between the two peaks is

3.72 eV. Consistent with zero-valent Au, the XPS binding energy of Au 4f_{7/2} confirmed the presence of Au (0) based on the peaks observed [13,18]. It is important to mention that the spectrum lacked the typical characteristic peaks associated with Au(III), suggesting a thorough reduction of Au(III) to Au(0) during the preparation reaction. The completed reduction of Au(III) is due to an excess of reducing agent NaBH₄. Gold nanoparticles were visible-light-induced synthesized using Lantana camara flower extract, which has good antibacterial activity. The gap between Au 4f_{7/2} and Au 4f_{5/2} is also 3.7 eV [19]. The XPS survey spectra manifest that the surface elements of Au₂₀-Hb NPs were derived from bovine hemoglobin and HAuCl₄. Thus, the XPS measurements confirm the existence of zero-valent gold nanoparticles, which were stabilized by bovine hemoglobin.

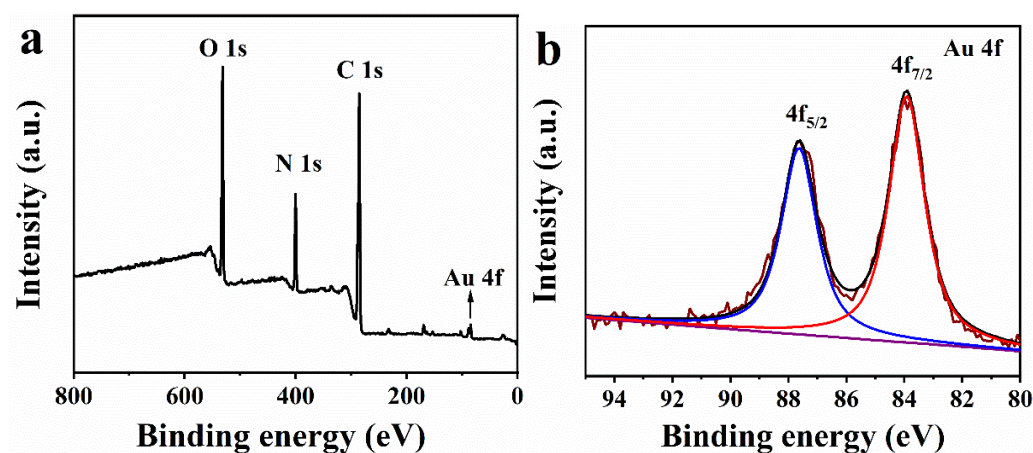


Figure 3. (a) XPS survey spectrum of Au₂₀-Hb NPs and (b) Au 4f binding energy analysis.

2.4. Stability in Solution

Basically, the size and dispersion state of Au NPs in an aqueous solution are the key factors for their catalytic activity. In order to evaluate the states of Au_n-Hb NPs, DLS was employed to measure the hydrodynamic size and zeta potential of Au_n-Hb NPs. As depicted in Figure 4a, the hydrodynamic size of bovine hemoglobin was 6.5 nm, and the hydrodynamic sizes of Au_n-Hb NPs (n = 20, 30, 40) were 7.5 nm, 8.7 nm, and 10.1 nm, respectively. It can be seen that Au_n-Hb NPs had a small hydrodynamic size. The hydrodynamic size of Au_n-Hb NPs also increases with the increasing amount of HAuCl₄ added. It should be noted that the hydrodynamic sizes of Au_n-Hb NPs were larger than the corresponding particle sizes shown in Figure 2. This was due to the different ways of preparing the samples. The Au_n-Hb NPs solution was deposited onto a carbon-coated copper grid and left to air dry overnight in preparation for the TEM technique, while the sample solution of Au_n-Hb NPs was measured in a hydration state for the DLS method. In addition, as we all know, the zeta potential plays a pivotal role in determining the strength of the mutual repulsion or attraction between nanoparticles in solution. The bigger of absolute value of the zeta potential of the nanoparticles, the more stable the nanoparticles in the solution. That is, a high zeta potential is good for resisting the aggregation of nanoparticles. In this experiment, the zeta potential of Au_n-Hb NPs (n = 20, 30, 40) was −1.0 mV for Au₂₀-Hb NPs, −21.3 mV for Au₃₀-Hb NPs, and −23.2 mV for Au₄₀-Hb NPs, as shown in Figure 4b. It shows that as the content of Au element in Au_n-Hb NPs increases, the absolute value of the zeta potential of Au_n-Hb NPs gets bigger. The pH values of Au₂₀-Hb NPs, Au₃₀-Hb NPs, and Au₄₀-Hb NPs were different. This should be the reason that the volume of the HAuCl₄ solution and NaBH₄ solution increased, which led to the pH of the mixture solution being slightly increased in the process of Au_n-Hb NP preparation. More carboxy groups of Au_n-Hb NPs were deprotonated with the increasing pH. Moreover, Au_n-Hb NPs remained stable without precipitation for at least four days, as shown in Figure 4c, while Au₂₀, Au₃₀, and Au₄₀ without bovine hemoglobin easily aggregated into large particles and formed precipitates, as shown in Figure 4d. The difference in Figure 4c,d

proved that the bovine hemoglobin had a positive influence on preventing self-aggregation of Au NPs during preparation and storage. The hydrophilic primary amine groups and carboxyl groups on the outside of the molecule keep bovine hemoglobin in a highly water-soluble state, which is conducive to maintaining its structural stability and exerting its functional properties. Hydrophilic bovine hemoglobin is good for the stability of Au_n -Hb NPs. The main contributing factors to the exceptional stability of Au_n -Hb NPs are electrostatic repulsion and steric hindrance.

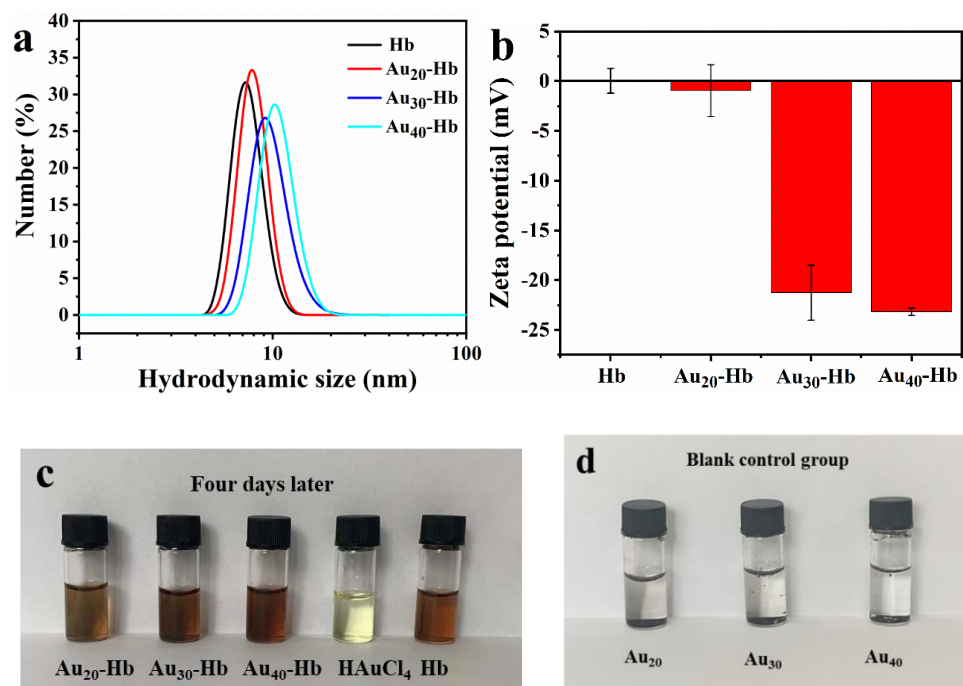


Figure 4. (a) Hydrodynamic size and (b) zeta potential of Au_n -Hb NPs. (c) Sample solution four days later and (d) blank control group. Au_{20} , Au_{30} , and Au_{40} mean gold nanoparticles without bovine hemoglobin.

2.5. Catalytic Performance

The catalytic performance of the synthesized Au_n -Hb NPs was quantitatively assessed by their ability to facilitate the reduction of 4-NP to 4-AP in the presence of an excess of $NaBH_4$ as the reducing agent. A time-dependent absorbance change in a mixed solution was monitored by UV-Vis spectra. As depicted in Figure 5a, the absorption peak observed at 317 nm corresponded to the pure 4-NP aqueous solution. Upon the introduction of $NaBH_4$, the absorption peak of 4-NP at 317 nm underwent a shift to 400 nm, demonstrating the formation of 4-nitrophenolate ions in the alkaline condition. The solution underwent a color alteration from transparent to intense yellow. Au_{20} -Hb NPs were picked up for further catalytic research. After the addition of the Au_{20} -Hb NPs, the absorption peak intensity of 4-nitrophenolate ions at 400 nm dramatically decreased, indicating the consumption of 4-nitrophenolate ions and the generation of 4-AP, as shown in Figure 5b. Moreover, the 4-NP conversion rate reached 98% after 21 min for Au_{20} -Hb NPs in Figure 5c, and the resulting solution became colorless. As depicted in Figure 5d, $\ln(C_t/C_0)$ versus reaction time (t) for the different amounts of Au_{20} -Hb NPs is linear. The catalytic performance of Au_{20} -Hb NPs was improved with increasing amounts of Au_{20} -Hb NPs. Furthermore, the catalytic reaction conformed to a pseudo-first-order kinetic equation in the presence of an excess of $NaBH_4$. (Equation (2)). C_t represents the concentration of 4-NP at time t , while C_0 denotes the initial concentration of 4-NP at $t = 0$, k_{app} is the rate constant (s^{-1}), and t is time.

$$\ln \frac{C_t}{C_0} = \ln \frac{A_t}{A_0} = -k_{app}t \quad (1)$$

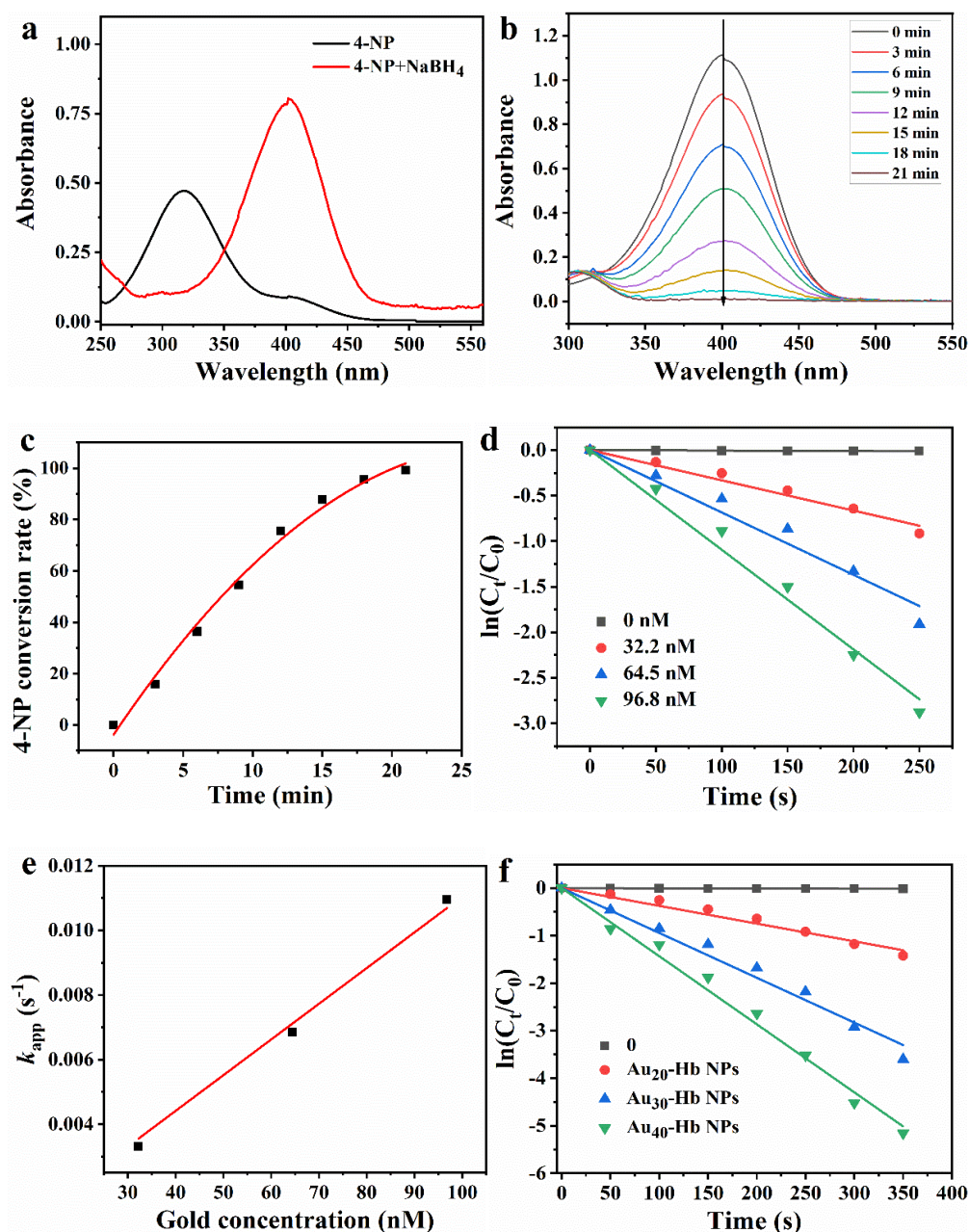


Figure 5. (a) UV-Vis spectra of 4-NP and 4-NP + NaBH₄, (b) UV-Vis spectra recorded for 4-NP + NaBH₄ following the addition of Au₂₀-Hb NPs every 3 min, (c) 4-NP conversion rate after the addition of Au₂₀-Hb NPs, (d) the correlation between ln(C_t/C₀) and the reaction time for different concentration of Au₂₀-Hb NPs, (e) k_{app} against different gold concentrations of Au₂₀-Hb NPs, and (f) the association between ln(C_t/C₀) and the elapsed reaction time for diverse Au_n-Hb NPs.

The k_{app} value is also linearly dependent on the amount of Au₂₀-Hb NPs in Figure 5e. It has been shown that the k_{app} value is related to mass transfer resistance, size of gold nanoparticles, temperature, and 4-NP, NaBH₄ [20], or catalyst concentration [21]. The k_{app} value increases with increasing temperature, NaBH₄, or catalyst concentration [20]. It has been reported that k_{app} decreases with increasing 4-NP concentration and increasing mass transfer resistance [20]. Increasing mass transfer resistance limits substrate contacts with

active metal sites on the catalyst. Here, the low k_{app} value of Au₂₀-Hb NPs should be due to their low concentration. In order to compare the effect of the n value on the catalytic activity of Au _{n} -Hb NPs, the same amount of Au _{n} -Hb NPs was added in the catalytic reduction process of 4-NP, where the hemoglobin concentration was the same. Figure 5f illustrates the linear relationship between $\ln(C_t/C_0)$ and time (t) during the catalytic reduction of Au _{n} -Hb NPs. As the number of gold nanoparticles on each hemoglobin molecule increased, the corresponding catalytic activity also increased. Au _{n} -Hb NPs exhibited a good catalytic reduction behavior, indicating that Au _{n} -Hb NPs were effective catalysts for the reduction of 4-NP.

Many groups reported the catalytic reduction of 4-NP by metal nanoparticles treated with NaBH₄ [22–25]. For a comparative evaluation of catalytic efficacy against alternative catalysts, calculations were performed for the normalized rate constant ($k_{nor} = k_{app}/n_{Au}$) and turnover frequency (TOF) of Au _{n} -Hb NPs. TOF is quantified as the ratio of the number of molecules generated by the reducing species 4-NP to the moles of catalytically active sites per hour when the 4-NP conversion achieves 90%. Table 1 shows the calculated k_{app} and TOF comparison of Au₂₀-Hb NPs in conjunction with catalysts mentioned in previous studies. Here, the TOF of Au₂₀-Hb NPs was determined to be 6768 h^{−1}, which was much higher than those of Au/graphene (12 h^{−1}), Au NPs (94 h^{−1}), GO@NH₂-Au NPs (595 h^{−1}), Au₁₀-LP (6053 h^{−1}), and Au/Fe₂O₃@HAP (241.3 h^{−1}). The k_{nor} of Au₂₀-Hb NPs was 3.32×10^4 s^{−1}mmol^{−1}, which was also much higher than those of GO@NH₂-Au NPs (5.85×10^2 s^{−1}mmol^{−1}), Au₁₀-LP (1.31×10^3 s^{−1}mmol^{−1}), Au/Fe₂O₃@HAP (1.27×10^3 s^{−1}mmol^{−1}), Au NPs/AOBC (2.98×10^3 s^{−1}mmol^{−1}), and Cu-Au BNSs (2.01×10^4 s^{−1}mmol^{−1}). Thus, Au₂₀-Hb NPs had superior activity in the catalytic reduction reaction of 4-NP. It should be noted that the size of the AuNPs inside Au _{n} -Hb NPs is smaller than most Au NPs in Table 1. The advantages of 4-NPs can be attributed to good stability and the small size of gold nanoparticles. It is well known that smaller Au NPs should have more active sites and higher catalytic activity. The specific surface area of Au₂₀-Hb NPs is quite high, and the elevated catalytic efficiency can primarily be attributed to the considerable specific surface area or high active site content for catalytic reactions on the gold nanoparticle surface. Gold nanoparticles that are small in size can also be stabilized by ligands. However, robust ligands may hinder the functioning of active surface sites, ultimately reducing catalytic ability. The Au NPs without ligands will precipitate for a long time, which also largely reduces their catalytic activity.

The reaction rate is very slow in kinetics without Au₂₀-Hb NPs. It can be concluded that Au₂₀-Hb NPs were effective catalysts for the reduction of 4-NP. The bovine hemoglobin acted as an excellent stabilizer for Au NPs. The absorption of BH₄[−] onto Au nanoparticles potentially provides Au–H species, which play a role in facilitating the transfer of all four electrons [1,26]. Many research groups have documented the mechanism involved in the catalytic reduction of 4-NP using noble metal nanoparticles under the conditions of NaBH₄ [26–28]. It is widely acknowledged that the catalytic reaction of 4-NP follows Langmuir–Hinshelwood kinetics. Ballauff et al. [29] proposed a detailed mechanism of the catalytic reaction. All compounds rapidly achieve equilibrium between adsorption and desorption. 4-NP is first rapidly converted to the stable intermediate (4-Hx). The concentration of 4-Hx remains approximately constant without catalysts. The intermediate 4-Hx is further reduced to form 4-AP after the addition of catalysts, which is the rate-determining step in the kinetic process [30].

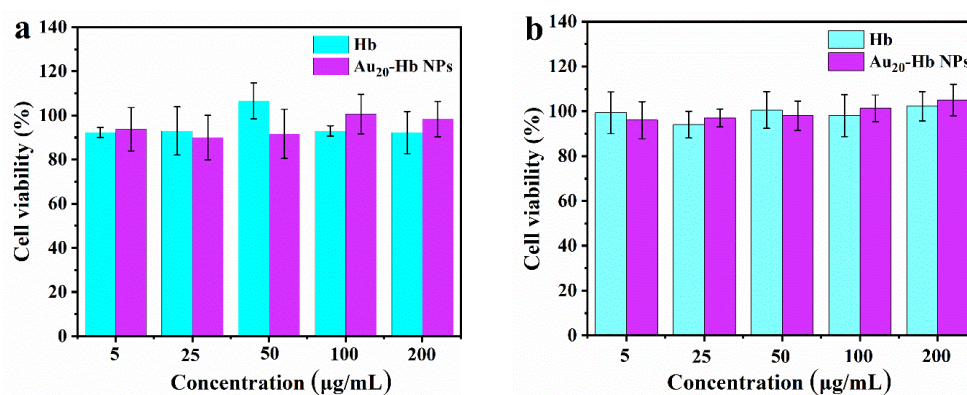
It is expected that the catalytic reaction facilitated by Au₂₀-Hb NPs also adheres to Langmuir–Hinshelwood kinetics. All the components in this reaction quickly reach an adsorption/desorption equilibrium on the surface of gold nanoparticles of Au₂₀-Hb NPs. The rate-determining step is the formation of 4-AP, which occurred only on the surface of the gold nanoparticles.

Table 1. Comparative analysis of k_{nor} and TOF values for Au₂₀-Hb NPs with other catalysts.

Catalyst	Au Size (nm)	k_{app} ($\times 10^{-3} \text{ s}^{-1}$)	k_{nor} ($\text{s}^{-1} \text{ mmol}^{-1}$)	TOF (h^{-1})	Ref.
Au ₂₀ -Hb	1.4	3.32	3.32×10^4	6768	This work
Au/graphene	14.6	3.17	6.25	12	[31]
Au NPs	80	7.42	1.46×10^2	94	[23]
GO@NH ₂ -Au NPs	14	35.6	5.85×10^2	595	[32]
Au ₁₀ -LP	7.8	4.65	1.31×10^3	6053	[33]
Au/Fe ₂ O ₃ @HAP	10	7.12	1.27×10^3	241.3	[34]
Au NPs/AOBC	10.6	4.47	2.98×10^3	1198	[35]
Cu-Au BNSs	78	30.2	2.01×10^4	536.4	[36]

2.6. Biocompatibility

The catalysts have good catalytic ability with regard to the degradation of organic pollutants, and they also should be biocompatible with our body. MTT is a widely accepted method to measure the cytotoxicity of nanomaterials [37]. Bovine hemoglobin is a kind of biocompatible biomolecule in the body. Here, the MTT assay was employed to determine the cytotoxicity of bovine hemoglobin and Au₂₀-Hb NPs against HeLa cells and A549 cells. Cell viability exceeded 90% when the concentration of Au₂₀-Hb NPs and bovine hemoglobin was lower than 200 $\mu\text{g}/\text{mL}$, as illustrated in Figure 6. Thus, Au₂₀-Hb NPs and bovine hemoglobin were biocompatible towards cells. The good biocompatibility should be due to biocompatible bovine hemoglobin. Bovine hemoglobin has the function of transporting nutrients and oxygen and emitting carbon dioxide in the body. Compared with highly toxic PEI, Au₂₀-Hb NPs can be applied well in bio-related catalysis.

**Figure 6.** Cell viability of (a) HeLa cells and (b) A549 cells for bovine hemoglobin and Au₂₀-Hb NPs.

3. Materials and Methods

3.1. Materials

Bovine hemoglobin (Hb) from bovine blood, chloroauric acid (HAuCl₄), sodium borohydride (NaBH₄), 4-nitrophenol (4-NP), and dimethyl sulfoxide (DMSO) were bought from Aladdin. HeLa cells and A549 cells were purchased from the China Center for Typical Culture Collection.

3.2. Synthesis of Au_n-Hb NPs

A total of 32 mg of bovine hemoglobin was dissolved in 10 mL of deionized water to obtain 0.05 mM of the bovine hemoglobin solution. Then, 2 mM of the HAuCl₄ solution at different volumes (200 μL , 300 μL , 400 μL) was mixed with 400 μL of the prepared bovine hemoglobin solution, respectively. The molar ratio of HAuCl₄ to bovine hemoglobin was 20:1, 30:1, and 40:1, respectively. The mixed solution was kept at 25 °C in a constant temperature mixer (600 rpm) for 15 min. The freshly prepared NaBH₄ (1 mg/mL) with

an equal volume to the HAuCl_4 solution was added rapidly, respectively. The solution underwent a color change from yellow to dark red, suggesting the formation of $\text{Au}_n\text{-Hb}$ NPs ($n = 20, 30, 40$). The sample was stored at 4°C for further experiments.

3.3. Characterization of $\text{Au}_n\text{-Hb}$ NPs

The UV-Vis spectra of hemoglobin and the $\text{Au}_n\text{-Hb}$ NP solution were acquired by a UV-vis spectrophotometer (TU-1810PC). The hydrodynamic size and zeta potential of $\text{Au}_n\text{-Hb}$ NPs were measured three times using a dynamic light scattering (DLS) measurement from Zetasizer (Nano ZS90). The software for Nano ZS90 is Zetasizer version 7.11. X-ray photoelectron spectroscopy (XPS) spectra were performed on a Thermo Scientific EACALAB 250Xi. The sample for XPS was dialyzed and lyophilized. The size and shape of $\text{Au}_n\text{-Hb}$ NPs were analyzed using transmission electron microscopy (TEM, HT 7700). $\text{Au}_n\text{-Hb}$ NPs were immobilized onto a carbon-coated copper grid and left to dry overnight prior to measurement. The software used was Nano Measurer version 1.2, which counted Au nanoparticles to determine the size distribution.

3.4. Catalytic Performance of $\text{Au}_n\text{-Hb}$ NPs

$\text{Au}_n\text{-Hb}$ NPs were employed to catalytically reduce 4-NP, following a procedure based on prior reports with slight alterations.

(1) The merging of a 4-NP aqueous solution (0.1 mM, 2 mL) and freshly prepared NaBH_4 (0.5 M, 1 mL) occurred in a quartz cuvette at room temperature. Then, $\text{Au}_{20}\text{-Hb}$ NPs (100 μL) were added into the mixture solution, with UV-Vis spectra monitoring the reaction solution every 3 min.

(2) In situ 4-NP reduction by NaBH_4 occurred by mixing the 4-NP (0.1 mM, 2 mL) aqueous solution and fresh NaBH_4 (0.5 M, 1 mL) in a quartz cuvette. Then, $\text{Au}_n\text{-Hb}$ NPs (100–400 μL) were added. In situ measurement of the absorbance at 403 nm in a mixed solution was conducted using a UV-Vis spectrophotometer.

3.5. MTT Assay

The cytotoxicity of HeLa cells and A549 cells were inoculated into 96-well culture plates (1×10^4 cells/well). After 24 h, the DMEM medium supplemented with 10% fetal bovine serum was exchanged with a fresh DMEM medium containing the samples (hemoglobin and $\text{Au}_{20}\text{-Hb}$ NPs) from 5 to 200 $\mu\text{g}/\text{mL}$. After 24 h, the cells were treated with a new 100 μL DMEM medium containing 500 $\mu\text{g}/\text{mL}$ MTT. After 4 h, the MTT solution was aspirated and substituted with 150 μL of DMSO. The absorbance (A) value at 490 nm was measured with a microplate reader. Cell viability was assessed using Formula (1). A_{sample} means the absorbance value of the sample, and A_{control} means the absorbance value of the control group.

$$\text{Cell viability (\%)} = \frac{A_{\text{sample}}}{A_{\text{control}}} \times 100 \quad (2)$$

4. Conclusions

In conclusion, biocompatible and stable $\text{Au}_n\text{-Hb}$ NPs were prepared by a simple method. Bovine hemoglobin played an important role in stabilizing Au NPs. The Au NPs were well-dispersed with a small size of about 1.4–2.4 nm. $\text{Au}_n\text{-Hb}$ NPs exhibited good stability for at least four days. In addition, $\text{Au}_n\text{-Hb}$ NPs were good catalysts for the catalytic reduction of hazardous 4-NP. The catalytic kinetics follow the pseudo-first-order kinetic equation. The TOF and k_{nor} of $\text{Au}_{20}\text{-Hb}$ NPs were 6768 h^{-1} and 3.32×10^4 , which were much higher than those of other catalysts. More importantly, $\text{Au}_n\text{-Hb}$ NPs exhibited no cytotoxicity towards cells. The prepared catalysts will have a good aspect in the treatment of phenolic pollutants.

Author Contributions: Methodology, N.Y.; investigation, Y.C. and S.L.; resources, X.Y. and L.W.; writing—original draft, Y.C.; writing—review and editing, N.Y., X.J. and L.W. All authors have read and agreed to the published version of the manuscript.

Funding: This research was supported by the Science Research Project of Hebei Education Department (QN2022124).

Data Availability Statement: The data presented in this study are available upon request from the corresponding author.

Conflicts of Interest: The authors declare no conflicts of interest.

References

1. Mejía, Y.R.; Bogireddy, N.K.R. Reduction of 4-nitrophenol using green-fabricated metal nanoparticles. *RSC Adv.* **2022**, *12*, 18661–18675. [[CrossRef](#)] [[PubMed](#)]
2. Shu, F.; Wu, J.; Jiang, G.; Qiao, Y.; Wang, Y.; Wu, D.; Zhong, Y.; Zhang, T.; Song, J.; Jin, Y.; et al. A hierarchically porous and hygroscopic carbon-based catalyst from natural wood for efficient catalytic reduction of industrial high-concentration 4-nitrophenol. *Sep. Purif. Technol.* **2022**, *300*, 121823. [[CrossRef](#)]
3. Chen, C.-S.; Chen, T.-C.; Chiu, K.-L.; Wu, H.-C.; Pao, C.-W.; Chen, C.-L.; Hsu, H.-C.; Kao, H.-M. Silver particles deposited onto magnetic carbon nanofibers as highly active catalysts for 4-nitrophenol reduction. *Appl. Catal. B* **2022**, *315*, 121596. [[CrossRef](#)]
4. Hu, C.; Yang, C.; Wang, X.; Wang, X.; Zhen, S.; Zhan, L.; Huang, C.; Li, Y. Rapid and facile synthesis of Au nanoparticle-decorated porous MOFs for the efficient reduction of 4-nitrophenol. *Sep. Purif. Technol.* **2022**, *300*, 121801. [[CrossRef](#)]
5. Ermis, S.; Kaya, K.; Topuz, F.; Yagci, Y. In-Situ and green photosynthesis of PVP-stabilized palladium nanoparticles as efficient catalysts for the reduction of 4-nitrophenol. *Inorg. Chem. Commun.* **2023**, *152*, 110626. [[CrossRef](#)]
6. Li, Q.; Zhou, H.; Li, G.Y.; Ye, Y.X.; Xia, D.S. Efficient catalytic reduction of 4-nitrophenol by magnetic Cu/Fe nanocomposite catalyst. *Desalin. Water Treat.* **2022**, *272*, 138–143.
7. Xia, W.; Zhao, F.; Fang, P.; An, M.; Zhu, J.; Cheng, K.; Xia, M. Magnetic Fe₃O₄@C nanoparticles separated from cold rolling mill sludge for 4-nitrophenol reduction. *Sep. Purif. Technol.* **2023**, *309*, 123018. [[CrossRef](#)]
8. He, H.; Tao, G.; Wang, Y.; Cai, R.; Guo, P.; Chen, L.; Zuo, H.; Zhao, P.; Xia, Q. In situ green synthesis and characterization of sericin-silver nanoparticle composite with effective antibacterial activity and good biocompatibility. *Mater. Sci. Eng. C* **2017**, *80*, 509–516. [[CrossRef](#)]
9. Nogueira, S.S.; de Araujo-Nobre, A.R.; Mafud, A.C.; Guimarães, M.A.; Alves, M.M.M.; Plácido, A.; Carvalho, F.A.A.; Arcanjo, D.D.R.; Mascarenhas, Y.; Costa, F.G.; et al. Silver nanoparticle stabilized by hydrolyzed collagen and natural polymers: Synthesis, characterization and antibacterial-antifungal evaluation. *Int. J. Biol. Macromol.* **2019**, *135*, 808–814. [[CrossRef](#)]
10. San, B.H.; Moh, S.H.; Kim, K.K. The effect of protein shells on the antioxidant activity of protein-encapsulated platinum nanoparticles. *J. Mater. Chem.* **2012**, *22*, 1774–1780. [[CrossRef](#)]
11. Li, R.; Zhao, Y.; Zhang, T.; Ju, Z.; Ji, X.; Cui, Y.; Wang, L.; Xiao, H. Pd nanoparticles stabilized by bitter melon polysaccharide with peroxidase properties for H₂O₂ detection. *Int. J. Biol. Macromol.* **2023**, *233*, 123513. [[CrossRef](#)] [[PubMed](#)]
12. Li, R.; He, M.; Cui, Y.; Ji, X.; Zhang, L.; Lan, X.; Wang, L.; Han, Z.; Xiao, H. Silver-palladium bimetallic nanoparticles stabilized by elm pod polysaccharide with peroxidase-like properties for glutathione detection and photothermal anti-tumor ability. *Int. J. Biol. Macromol.* **2024**, *264*, 130673. [[CrossRef](#)] [[PubMed](#)]
13. Noël, S.; Bricout, H.; Addad, A.; Sonnendecker, C.; Zimmermann, W.; Monflier, E.; Léger, B. Catalytic reduction of 4-nitrophenol with gold nanoparticles stabilized by large-ring cyclodextrins. *New J. Chem.* **2020**, *44*, 21007–21011. [[CrossRef](#)]
14. Pestovsky, Y.S.; Martinez-Antonio, A. Synthesis of gold nanoparticles by tetrachloroaurate reduction with cyclodextrins. *Química Nova* **2018**, *41*, 926–932. [[CrossRef](#)]
15. Stiufluic, G.; Toma, V.; Moldovan, A.I.; Stiufluic, R.; Lucaci, C.M. One pot microwave assisted synthesis of cyclodextrins capped spherical gold nanoparticles. *Dig. J. Nanomater. Biostruct.* **2017**, *12*, 1089–1095.
16. Faggiano, S.; Ronda, L.; Bruno, S.; Abbruzzetti, S.; Viappiani, C.; Bettati, S.; Mozzarelli, A. From hemoglobin allosterity to hemoglobin-based oxygen carriers. *Mol. Asp. Med.* **2022**, *84*, 101050. [[CrossRef](#)] [[PubMed](#)]
17. Balasco, N.; Alba, J.; D'abramo, M.; Vitagliano, L. Quaternary structure transitions of human hemoglobin: An atomic-level view of the functional intermediate states. *J. Chem. Inf. Model.* **2021**, *61*, 3988–3999. [[CrossRef](#)]
18. Fu, Y.; Xu, P.; Huang, D.; Zeng, G.; Lai, C.; Qin, L.; Li, B.; He, J.; Yi, H.; Cheng, M.; et al. Au nanoparticles decorated on activated coke via a facile preparation for efficient catalytic reduction of nitrophenols and azo dyes. *Appl. Surf. Sci.* **2019**, *473*, 578–588. [[CrossRef](#)]
19. Hidayat, H.; Purwiandono, G.; Tohari, T.; Nugroho, B.H.; Jauhari, M.H.; Widyaputra, S.B.; Fatimah, I. Antibacterial and photocatalytic activity of visible-light-induced synthesized gold nanoparticles by using *Lantana camara* flower extract. *Green Process. Synth.* **2022**, *11*, 1072–1082. [[CrossRef](#)]
20. Nemanashi, M.; Meijboom, R. Synthesis and characterization of Cu, Ag and Au dendrimer-encapsulated nanoparticles and their application in the reduction of 4-nitrophenol to 4-aminophenol. *J. Colloid Interface Sci.* **2013**, *389*, 260–267. [[CrossRef](#)]

21. Bingwa, N.; Meijboom, R. Evaluation of catalytic activity of Ag and Au dendrimer-encapsulated nanoparticles in the reduction of 4-nitrophenol. *J. Mol. Catal. A Chem.* **2015**, *396*, 1–7. [[CrossRef](#)]
22. Dai, Y.; Li, Y.; Wang, S. ABC triblock copolymer-stabilized gold nanoparticles for catalytic reduction of 4-nitrophenol. *J. Catal.* **2015**, *329*, 425–430. [[CrossRef](#)]
23. Guo, M.; He, J.; Li, Y.; Ma, S.; Sun, X. One-step synthesis of hollow porous gold nanoparticles with tunable particle size for the reduction of 4-nitrophenol. *J. Hazard. Mater.* **2016**, *310*, 89–97. [[CrossRef](#)] [[PubMed](#)]
24. Shen, W.; Qu, Y.; Pei, X.; Li, S.; You, S.; Wang, J.; Zhang, Z.; Zhou, J. Catalytic reduction of 4-nitrophenol using gold nanoparticles biosynthesized by cell-free extracts of *Aspergillus* sp. WL-Au. *J. Hazard. Mater.* **2017**, *321*, 299–306. [[CrossRef](#)] [[PubMed](#)]
25. Nasrollahzadeh, M.; Sajjadi, M.; Irvani, S.; Varma, R.S. Green-synthesized nanocatalysts and nanomaterials for water treatment: Current challenges and future perspectives. *J. Hazard. Mater.* **2021**, *401*, 123401. [[CrossRef](#)]
26. Liu, C.; Li, G.; Ma, E.; Zeng, F.; Wu, T.; Chen, K.; Fan, P.; Wen, X.; Li, L.; Qu, Q. Control-synthesized ultrafine Au nanoparticles by *Aspergillus niger* extracellular metabolites from SIM cards as high-effective 4-nitrophenol degradation catalyst. *J. Environ. Chem. Eng.* **2022**, *10*, 108676. [[CrossRef](#)]
27. Liu, X.; Liu, F. Bimetallic (AuAg, AuPd and AgPd) nanoparticles supported on cellulose-based hydrogel for reusable catalysis. *Carbohydr. Polym.* **2023**, *310*, 120726. [[CrossRef](#)]
28. Deshmukh, A.R.; Dikshit, P.K.; Kim, B.S. Green in situ immobilization of gold and silver nanoparticles on bacterial nanocellulose film using *Punica granatum* peels extract and their application as reusable catalysts. *Int. J. Biol. Macromol.* **2022**, *205*, 169–177. [[CrossRef](#)] [[PubMed](#)]
29. Gu, S.; Wunder, S.; Lu, Y.; Ballauff, M.; Fenger, R.; Rademann, K.; Jaquet, B.; Zaccone, A. Kinetic analysis of the catalytic reduction of 4-nitrophenol by metallic nanoparticles. *J. Phys. Chem. C* **2014**, *118*, 18618–18625. [[CrossRef](#)]
30. Wang, L.; Qiang, X.; Song, Y.; Wang, X.; Gu, W.; Niu, J.; Sun, Y.; Srinuanpan, S.; Wang, G. Green synthesis of gold nanoparticles by phycoerythrin extracted from *Solieria tenuis* as an efficient catalyst for 4-nitrophenol reduction and degradation of dyes in wastewater. *Mater. Today Sustain.* **2023**, *23*, 100435. [[CrossRef](#)]
31. Li, J.; Liu, C.-Y.; Liu, Y. Au/graphene hydrogel: Synthesis, characterization and its use for catalytic reduction of 4-nitrophenol. *J. Mater. Chem.* **2012**, *22*, 8426–8430. [[CrossRef](#)]
32. Ju, Y.; Li, X.; Feng, J.; Ma, Y.; Hu, J.; Chen, X. One pot in situ growth of gold nanoparticles on amine-modified graphene oxide and their high catalytic properties. *Appl. Surf. Sci.* **2014**, *316*, 132–140. [[CrossRef](#)]
33. Zhang, X.; Fan, L.; Cui, Y.; Cui, T.; Chen, S.; Ma, G.; Hou, W.; Wang, L. Green synthesis of gold nanoparticles using longan polysaccharide and their reduction of 4-nitrophenol and biological applications. *Nano* **2020**, *15*, 2050002. [[CrossRef](#)]
34. Xia, Y.; Liu, Y.; Shi, N.; Zhang, X. Highly efficient reduction of 4-nitrophenolate to 4-aminophenolate by Au/-Fe₂O₃@HAP magnetic composites. *RSC Adv.* **2019**, *9*, 10272–10281. [[CrossRef](#)] [[PubMed](#)]
35. Chen, M.; Kang, H.; Gong, Y.; Guo, J.; Zhang, H.; Liu, R. Bacterial cellulose supported gold nanoparticles with excellent catalytic properties. *ACS Appl. Mater. Interfaces* **2015**, *7*, 21717–21726. [[CrossRef](#)] [[PubMed](#)]
36. Guan, Y.; Fu, S.; Song, W.; Zhang, X.; Liu, B.; Zhang, F.; Chai, F. Controllable synthesis of sea urchin-like Cu-Au bimetallic nanospheres and their utility as efficient catalyst for hydrogenation of 4-nitrophenol. *J. Solid State Chem.* **2023**, *322*, 123968. [[CrossRef](#)]
37. Zi, W.; Karmakar, B.; El-kott, A.F.; Al-Saeed, F.A.; Negm, S.; Salem, E.T. Green synthesized silver nanoparticles incorporated graphene oxide: Investigation of its catalytic activity, antioxidant and potential activity against colorectal cancer cells. *J. Inorg. Organomet. Polym. Mater.* **2023**, *33*, 1693–1703. [[CrossRef](#)]

Disclaimer/Publisher's Note: The statements, opinions and data contained in all publications are solely those of the individual author(s) and contributor(s) and not of MDPI and/or the editor(s). MDPI and/or the editor(s) disclaim responsibility for any injury to people or property resulting from any ideas, methods, instructions or products referred to in the content.